Human-Robot Shared Visual Servoing Based on Game Theory

Zitai Fang#, Chong Cao# and Lijun Han*

***Abstract*— Human-robot shared visual servoing systems can combine the precise control ability of the robot and the human decision-making ability. However, integrating human input into such systems remains a challenging endeavor. This work studies the robot visual servoing control system in the human-robot shared environment and proposes a human-robot shared visual servoing framework based on game theory. Game theory is used to model the relationship between humans and robots. According to the observation of human input, the human intention is adaptively estimated using a radial basis function neural network (RBFNN), and the robot control objective is dynamically adjusted to realize human-robot coordination. The Lyapunov theory is used to prove the stability of the system. Experiments are conducted to verify the effectiveness of the proposed method.**

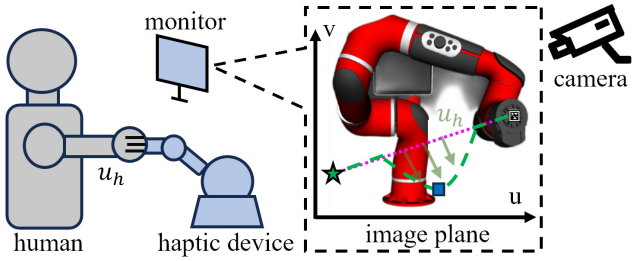

Fig. 1. Concept of the proposed human-robot shared visual servoing system. The pink dotted line represents the prescribed trajectory, the green dotted line represents the actual trajectory, the blue square represents human desired position, and the green star represents the target point.

I. INTRODUCTION

Physical human-robot interaction (pHRI) has been widely applied in many fields, such as wearable devices, welding, remote assembly, et al. [1]–[3]. Owing to the lightweight and cheapness of monocular cameras, monocular visual servoing technology is still one of the most active research directions [4]. Thus, a system simultaneously exploiting visual servoing and human-robot interaction information is worthy of discussion. We refer to this system as the human-robot shared visual servoing system. However, integrating human input into visual servoing systems remains a challenging endeavor.

Conventional human-robot shared visual servoing systems always consider a fixed "co-activity" (definition in [5]) relationship between humans and robots. In [6] and [7], different degrees of gripper freedom are allocated to humans and robots. Visual servoing is exploited to guide the robot to the target grasping positions while the human handles other subtasks like moving assembly parts. In [8], the human actively participates in a plug assembly task by holding the socket while the robot tracks the plug using visual servoing. In these articles, task is divided into subtasks and allocated to humans and robots. Unlike a fixed "co-activity" relationship, [9], [10] treat the robot as a "follower" in a human-robot co-carrying scenario, with the human acting as the leader. This is a classic "leader/follower" paradigm. The robot estimates the human intention using visual information and actively follows the human's lead. Visual servoing is exploited to generate a reference trajectory for the impedance controller. In the above works, the relationship in the human-robot shared visual servoing systems is fixed. Compared to the fixed relationship, which may heighten the burden of human decision-making, the dynamic role adaption relationship (i.e., adjustable leader/follower roles) can offer more advantages in the process of human-robot collaboration [11], [12].

The human-robot interaction system is equal to a dual-agent system. Game theory is highly effective in addressing the control and decision-making tasks of multi-agent systems [13], thus, it has been widely used in the field of human-robot interaction recently [14]–[16]. The game theory-based controller has been proved effective in modeling human-robot relationship [17]. [18] uses game theory to settle the bargaining problem in human-robot role arbitration, which can be integrated with different control modules. In [19], considering a linear system differential game, the Nash equilibrium is used to describe the optimal control between humans and robots. The linear system is typically considered in these works. When using a monocular camera for image-based visual servoing, the image depth leads to non-linearity of the system, which brings a great challenge for modeling a human-robot collaboration system. [20] provides a general framework for dealing with different kinds of systems. Verification experiments are performed on a 2D plane instead of a non-linear 3D configuration scene. We aim to design a game theory-based controller for the non-linear visual servoing system.

We notice that there is a lack of research on human-robot shared visual servoing systems to realize dynamic role adaption. Thus, in this work, we study the robot visual servoing control system in the human-robot shared environment. We design a game theory-based controller for dynamic

This work was supported in part by the National Key R&D Program of China (Grant No.2023YFB4705700), in part by the Natural Science Foundation of China under 62403311, in part by China Postdoctoral Science Foundation 2025T180468, GZC20231590 and 2024M761972. (Corresponding Author: Lijun Han)

Z. T. Fang, C. Chong and L. J. Han are with School of Automation and Intelligent Sensing, Shanghai Jiao Tong university and State Key Laboratory of Avionics Integration and Aviation System-of-Systems Synthesis, Shanghai 200240, China. (e-mail: fangzitai@sjtu.edu.cn, cxls1534826624w@sjtu.edu.cn, lijun_han@sjtu.edu.cn)

# These authors have contributed equally to this work.

role adaption and a radial basis function neural network for human intention estimation. Furthermore, we demonstrate the effectiveness of our approach both theoretically and experimentally with a non-linear 3D configuration scene.

To sum up, we highlight our contributions as follows.

- A shared controller based on game theory is proposed for the human-robot shared visual servoing systems, enabling dynamic role adaption by online adjusting the robot's control objective and output.
- A radial basis function neural network is employed to estimate human intention online and address the inherent non-linearity of the visual servoing system.
- The stability of the system is theoretically proven by the Lyapunov theory and further validated through experiments.

II. Problem Formulation

A. System Description

The human-robot shared visual servoing system is shown in Fig. 1, allowing humans to participate in visual servoing. The feature point is selected at the robot's end-effector as the visual feature. In this scenario, the feature point is expected to track a prescribed trajectory when there is no human participation, and the robot takes the lead to realize visual servoing. While the human achieves physical interaction through the haptic device with visual feedback, the prescribed trajectory is adjusted to pass through the human desired position, which means that the human takes the lead to make a trajectory deformation. Such a scenario is also common in other tasks, like collaborative assembly and welding, where the human may take real-time corrective action to modify the prescribed trajectory. The considered visual servoing system is a monocular image-based system with an eye-to-hand setup. The pin-hole camera is fixed in front of the collaboration workbench, and the intrinsic and extrinsic parameters of the camera are known in advance.

We use vector $y(t) = \begin{bmatrix} u & v \end{bmatrix}^T$ to represent the coordinates of feature points and denote k as the number of feature points. Vector $x(t)$ is the coordinates of feature points in Cartesian space w.r.t robot base frame. Refer to [21] for the process of visual servoing system modeling using the perspective projection model, we have

$$\begin{bmatrix} y(t) \\ 1 \end{bmatrix} = \frac{1}{z(t)} P \begin{bmatrix} x(t) \\ 1 \end{bmatrix} \tag{1}$$

where $P \in \mathbb{R}^{3\times 4}$ is the perspective projection matrix. Scalar $z(t)$ is the depth of the feature point and is given by

$$z(t) = p_3^T x(t) + p_{34} \tag{2}$$

where $p_3^T = \begin{bmatrix} p_{31} & p_{32} & p_{33} \end{bmatrix}$ and p_{34} is a scalar. p_{ij} denotes the element in the i^{th} row and j^{th} column of the matrix P. By taking the derivative of (1), we have

$$\dot{y}(t) = \frac{1}{z(t)}(M\dot{x}(t) - y(t)\dot{z}(t)) \tag{3}$$

where $M = \begin{bmatrix} p_{11} & p_{12} & p_{13} \\ p_{21} & p_{22} & p_{23} \end{bmatrix}$. By taking the derivative of (3), we have

$$\ddot{y}(t) = -\frac{1}{z(t)}(\ddot{z}(t)y(t) + 2\dot{z}(t)\dot{y}(t) - M\ddot{x}(t)) \tag{4}$$

To integrate human input into the visual servoing systems, we exploit the impedance model in Cartesian space proposed in [22] and have

$$H_d\ddot{x}(t) + C_d\dot{x}(t) = u_r(t) + u_h(t) \tag{5}$$

where $H_d \in \mathbb{R}^{m\times m}$ and $C_d \in \mathbb{R}^{m\times m}$ are desired inertial and damping matrices, $u_r(t)$ and $u_h(t)$ are robot force and human force in Cartesian space, respectively. $\dot{x}(t)$ and $\ddot{x}(t)$ are the velocity and the acceleration, respectively. Define $y_d(t)$ as the prescribed trajectory of feature points, $\xi^{'} = [y^T \ \dot{y}^T]^T$ as the state and $\xi = [\xi^{'T} \ y_d{}^T]^T$ as the augmented state. Combine (1)(3)(4) and substitute into (5), then the state-space formulation of the human-robot shared visual servoing system is below

$$\dot{\xi} = h(\xi) + g_1(\xi)u_r + g_2(\xi)u_h \tag{6}$$

where

$$h(\xi) = \begin{bmatrix} A^{'}(\xi)\xi^{'} \\ \dot{y}_d \end{bmatrix} + h_0(\xi) \tag{7}$$

$$\begin{aligned} A^{'} &= \begin{bmatrix} -\frac{1}{z}p_3^T\dot{x}\mathbf{I}_{2k\times 2k} & \mathbf{0}_{2k\times 2k} \\ \frac{1}{z}p_3^T(H_d^{-1}C_d\dot{x})\mathbf{I}_{2k\times 2k} & -\frac{2}{z}p_3^T\dot{x}\mathbf{I}_{2k\times 2k} \end{bmatrix} \\ h_0 &= \begin{bmatrix} -\frac{1}{z}\dot{x}^TM^T & -\frac{1}{z}C_d^TH_d^{-T}\dot{x}^TM^T & \mathbf{0}_{1\times 2k} \end{bmatrix}^T \\ g_1 = g_2 &= \begin{bmatrix} \mathbf{0}_{m\times 2k} & \frac{1}{z}H_d^{-T}(M - yp_3^T)^T & \mathbf{0}_{m\times 2k} \end{bmatrix}^T \end{aligned} \tag{8}$$

and $\mathbf{0}_{i\times j}, \mathbf{I}_{i\times j}$ respectively denote $i \times j$ zero, identity matrices. Referring to (6)(7)(8), we know the system is a non-linear time-varying system.

B. Problem Formulation

Owing to the collaborative relationship between the human and the robot, it is reasonable to set the robot's cost function the same as the human's. The cost function is defined as

$$L = \int_0^{+\infty} c(t)dt \tag{9}$$

$$\begin{aligned} c(t) &= (y - y_d)^TQ_1(y - y_d) + \dot{y}^TQ_2\dot{y} + u_r^TR_1u_r + u_h^TR_2u_h \\ &= \xi^TQ\xi + u_r^TR_1u_r + u_h^TR_2u_h \end{aligned} \tag{10}$$

$$Q = \begin{bmatrix} Q_1 & \mathbf{0}_{2k\times 2k} & -Q_1 \\ \mathbf{0}_{2k\times 2k} & Q_2 & \mathbf{0}_{2k\times 2k} \\ -Q_1 & \mathbf{0}_{2k\times 2k} & Q_1 \end{bmatrix} \tag{11}$$

where L and c are the cost function and instantaneous cost function, $Q_1 \in \mathbb{R}^{2k\times 2k}$, $Q_2 \in \mathbb{R}^{2k\times 2k}$, $R_1 \in \mathbb{R}^{m\times m}$, $R_2 \in \mathbb{R}^{m\times m}$ are positive definite matrices, respectively the tracking error weight, the velocity regulation weight, the robot control weight and the human control weight. A higher R_1 means a higher penalty to the robot control and a higher tendency for the human to lead the task. Conversely, a higher

R_2 means a higher penalty for the human control and a higher tendency for the robot to lead the task.

Problem: *In a visual servoing system involving human participation, given the prescribed trajectory y_d of the feature points y on the image plane, design a control input u_r such that the feature points y track the prescribed trajectory y_d when there is no human input u_h (i.e., $u_h = 0$), and the robot coordinates with the human to move on a new trajectory when there exists human input u_h (i.e., $u_h \neq 0$) considering the minimization of human cost function L.*

III. Method

A. Game Theory

In this section, game theory is used to model the human-robot relationship. In game theory, there exist many types of equilibrium points, and we focus on the Nash equilibrium. When the Nash equilibrium is achieved between the human and the robot, it means that, given the strategy of the other, neither party can improve their outcome by unilaterally changing their strategy [23]. In other words, at Nash equilibrium, both the human and the robot are making optimal decisions based on each other's actions, leading to a stable and mutually beneficial collaboration. In the Stackelberg equilibrium, one agent aims to minimize its own cost function, while the other agent does not prioritize its own cost function but instead considers the cost function of the first agent. This results in a fixed "leader-follower" paradigm, which is not expected in our considered human-robot shared visual servoing system. As described in Section II, we hope that both the human and the robot can take the lead in different situations, meaning an adjustable leader/follower role, and the Nash equilibrium suits our design requirements.

As for how to solve the Nash equilibrium of nonlinear systems, an online adaptive learning method with policy iteration is applied [24]. Consider the system described by (6)(7)(8), to achieve the Nash equilibrium, the Hamiltonian function is first defined as

$$H(\nabla L, \xi, u_r, u_h) = c + \nabla L^T (h(\xi) + g_1(\xi)u_r + g_2(\xi)u_h) \tag{12}$$

Considering the optimal control condition, the control objective can be described as

$$L^*(\xi) = \min_{u_r, u_h} \int_t^{+\infty} (\xi^T Q \xi + u_r^T R_1 u_r + u_h^T R_2 u_h) d\mu \tag{13}$$

and satisfies the coupled Hamilton–Jacobi–Bellman equation

$$\min_{u_r, u_h} H^*(\nabla L, \xi, u_r, u_h) = 0 \tag{14}$$

Considering (9)(10)(11),we have the Nash equilibrium as

$$u_r^* = -\frac{1}{2} R_1^{-1} g_1^T \nabla L^*, \;\; u_h^* = -\frac{1}{2} R_2^{-1} g_2^T \nabla L^* \tag{15}$$

B. Controller Design

Due to the inherent uncertainty and immeasurability of the human cost function, the real human cost function needs to be estimated. In this section, an adaptive controller with RBFNN is designed to estimate human intention. For any

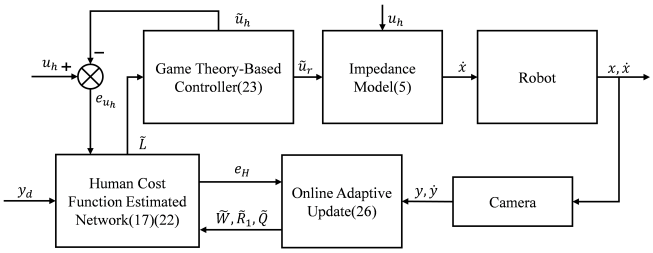

Fig. 2. Structure of the proposed control scheme (where the numbers in the brackets correspond to the equation labels).

variable ν, we define $\bar{\nu}$ as the ideal variable, $\tilde{\nu}$ as the estimated variable, e_ν as the error between $\bar{\nu}$ and $\tilde{\nu}$. The human cost function estimated by the neural network satisfies

$$\bar{L}(\xi) = \bar{W}^T \Phi(\xi) + \epsilon(\xi) \tag{16}$$

where $\bar{W}$ is the ideal neural network weight matrix, $\Phi(\xi)$ is the activation function, $\epsilon(\xi)$ is the approximation error. Due to the human cost function $\bar{L}(\xi)$ is immeasurable, the estimated human cost function is estimated as

$$\tilde{L} = \tilde{W}^T \Phi(\xi) \tag{17}$$

Also Assuming that the hidden layers of the network tend to be infinite, then, $\epsilon \to 0$. By taking the derivative of (16)(17), the ideal and estimated Hamiltonian function is defined as

$$\bar{H} = \bar{c} + \nabla \bar{L} = \bar{c} + \bar{W}^T \nabla \Phi(\xi) \dot{\xi} + \nabla \epsilon^T \dot{\xi} \tag{18}$$

$$\tilde{H} = \tilde{c} + \nabla \tilde{L} = \tilde{c} + \tilde{W}^T \nabla \Phi(\xi) \dot{\xi} \tag{19}$$

According to (14), $\bar{H}$ is equal to zero, then we have

$$-(\bar{c} + \bar{W}^T \Phi \dot{\xi}) = \nabla \epsilon^T \dot{\xi} := \epsilon_H \tag{20}$$

Since the weights in the instantaneous cost function are relative, we fix R_2 as a constant matrix, and the estimated instantaneous cost function can be written as

$$\tilde{c} = \xi^T \tilde{Q} \xi + \tilde{u}_r^T \tilde{R}_1 \tilde{u}_r + u_h^T R_2 u_h \tag{21}$$

Then e_H can be written as

$$e_H = \bar{H} - \tilde{H} = -(\tilde{W}^T \nabla \Phi \dot{\xi} + \xi^T \tilde{Q} \xi + u_r^T \tilde{R}_1 u_r + u_h^T R_2 u_h) \tag{22}$$

While the neural network converges, the following conditions should be satisfied

- The Nash equilibrium should be achieved, and the system is under optimal control. Namely, the error between $\bar{H}$ and $\tilde{H}$ should be minimized.
- The human intention (represented by the cost function) should be estimated correctly. Although the cost function is unknown, the actual force applied by the human is measurable. Specifically, the optimal human force has to track the actual human force to minimize the error between $\bar{c}$ and $\tilde{c}$.

Moreover, $\tilde{u}_r$ and $\tilde{u}_h$ satisfies (15) and are

$$\tilde{u}_r = -\frac{1}{2} \tilde{R}_1^{-1} g_1^T \nabla \Phi^T \tilde{W}, \;\; \tilde{u}_h = -\frac{1}{2} R_2^{-1} g_2^T \nabla \Phi^T \tilde{W} \tag{23}$$

$\tilde{u}_r$ in (23) is the output of the game theory-based controller and the input of the impedance model. Then, to online update weights $\tilde{W}, \tilde{Q}$ and $\tilde{R}_1$ to achieve network convergence and human intention estimation, the loss function of the network can be designed as

$$V = \frac{1}{2}e_H^T e_H + \frac{\beta}{2}\, e_{u_h}^T e_{u_h} \tag{24}$$

According to (23), e_{u_h} can be given as

$$e_{u_h} = u_h - \tilde{u}_h = u_h + \frac{1}{2}R_2^{-1}g_2^T\nabla\Phi^T\tilde{W} \tag{25}$$

The update rules using the gradient descent method are

$$\begin{aligned}\frac{\partial V}{\partial \tilde{W}} &= \tilde{W} + \alpha_1\nabla\Phi\dot{\xi}e_H - \alpha_1\frac{\beta}{2}\nabla\Phi g_2 R_2^{-T}e_{u_h}\\ \frac{\partial V}{\partial \tilde{Q}} &= \tilde{Q} + \alpha_2\xi^T\xi e_H, \frac{\partial V}{\partial \tilde{R}_1} = \tilde{R}_1 + \alpha_3\tilde{u}_r^T\tilde{u}_r e_H\end{aligned} \tag{26}$$

where $\alpha_1, \alpha_2, \alpha_3, \beta$ are positive constants. Finally, we set the activation function as the Gaussian function $\Phi(\xi) = [\phi_1, \phi_2, \ldots, \phi_N]^T$, and have $\phi_i = e^{\frac{-(\xi-\lambda)(\xi-\lambda)^T}{\zeta^2}}$ $(i = 1, 2, \ldots, N)$, where N is the number of hidden layer neurons, λ and ζ are the center and the width of the Gaussian function. We set $\lambda = [y_d^T, \dot{y} + \rho(y - y_d), y_d^T]^T (\rho \geq 0)$. The whole framework of the controller is summarized in Fig. 2.

C. Stability Analysis

Theorem 1. Assume that $\theta(t) = [\nabla\Phi\dot{\xi}, \xi^T\xi, \tilde{u}_r^T\tilde{u}_r]^T$ is persistently exciting,i.e., there exist k_1, k_2, such that

$$k_1\mathbf{I} \leq \int_t^{t+\delta T}\theta\theta^T d\mu \leq k_2\mathbf{I} \tag{27}$$

and refers to [25], the network residual error $\epsilon_{net} = \frac{1}{4c_1}\epsilon_H^2 + \frac{\beta}{4c_2}\|\nabla\epsilon_{u_h}\|^2$ is bounded,i.e., $\epsilon_{net} \leq \epsilon_{max}$. Considering the controller output $\tilde{u}_r$ in (23) and the update rules in (26), e_W, e_Q and e_{R_1} are bounded.

Proof. Define the Lyapunov function as

$$\Psi = \frac{1}{2\alpha_1}e_W^T e_W + \frac{1}{2\alpha_2}e_Q^T e_Q + \frac{1}{2\alpha_3}e_{R_1}^T e_{R_1} \tag{28}$$

For convenience, let $e = [e_W, e_Q, e_{R_1}]^T$ and combine (20)(26), then the error dynamics can be given as

$$\begin{aligned}\dot{e}_W &= -\alpha_1\nabla\Phi\dot{\xi}(e^T\theta + \epsilon_H) + \frac{\alpha_1\beta}{2}\nabla\Phi g_2 R_2^{-T}e_{u_h}\\ \dot{e}_Q &= -\alpha_2\xi^T\xi\ (e^T\theta + \epsilon_H), \dot{e}_{R_1} = -\alpha_3\tilde{u}_r^T\tilde{u}_r\ (e^T\theta + \epsilon_H)\end{aligned} \tag{29}$$

Take the derivative of (28), we have

$$\begin{aligned}\dot{\Psi} &= \frac{1}{\alpha_1}e_W^T\dot{e}_W + \frac{1}{\alpha_2}e_Q\dot{e}_Q + \frac{1}{\alpha_3}e_{R_1}^T\dot{e}_{R_1}\\ &= -(e^T\theta)^2 - e^T\theta\epsilon_H + \frac{\beta}{2}e_W^T\nabla\Phi g_2 R_2^{-T}e_{u_h}\end{aligned} \tag{30}$$

According to the ideal network output (equation(16)), the ideal optimal human input is

$$\bar{u}_h = -\frac{1}{2}R_2^{-1}g_2^T\nabla\Phi^T\bar{W} + \nabla\epsilon_{u_h} \tag{31}$$

where $\nabla\epsilon_{u_h} = -\frac{1}{2}R_2^{-1}g_2^T\nabla\epsilon$. Combine (29)(30)(31), the derivative of the Lyapunov function has the form

$$\dot{\Psi} = -(e^T\theta)^2 - e^T\theta\epsilon_H + \beta\nabla\epsilon_{u_h}^T e_{u_h} - \beta\|e_{u_h}\|^2 \tag{32}$$

Young's inequality proposes that, there exist $c_1, c_2 \in (0, 1)$, such that

$$\begin{aligned}-e^T\theta\epsilon_H &\leq c_1(e^T\theta)^2 + \frac{1}{4c_1}\epsilon_H^2\\ \beta\nabla\epsilon_{u_h}^T e_{u_h} &\leq \beta c_2\|e_{u_h}\|^2 + \frac{\beta}{4c_2}\|\nabla\epsilon_{u_h}\|^2\end{aligned} \tag{33}$$

Then, we obtain

$$\dot{\Psi} \leq -(1 - c_1)(e^T\theta)^2 - \beta(1 - c_2)\|e_{u_h}\|^2 + \epsilon_{net} \tag{34}$$

Thus, (34) gives an effective practical bound for $e^T\theta$ and satisfies $e^T\theta > \sqrt{\frac{\epsilon_{max}}{1-c_1}}$. Based on [26], the supremacy can be given as

$$\|e\| \leq \frac{\sqrt{k_2\delta}}{k_1(1 - c_1)}(1 + 2k_2c_5\alpha_1)\epsilon_{max} \tag{35}$$

where c_5 is a positive constant of the order of 1.

IV. EXPERIMENTS

A. Experimental Setup

Consider a scenario of human-robot co-transportation. The robot needs to transport materials to a target place. In the normal case, given the target point and prescribed trajectory of the transportation task, the robot is able to complete this task alone. However, in some cases, due to the sudden need for these materials from other places(here we refer to these places as the human desired position), the human wants to change part of the materials' transportation target from the initial target point to the human desired position and applies force to move the robot away from the prescribed trajectory to the human desired position. After reaching the human desired position and placing part of the materials, the human releases the robot and applies no force. Then the robot continues to track the prescribed trajectory and places the remaining materials in the initial target point.

Inspired by the above scenario, we design the experiment as in Fig. 3. A 7-DOF Sawyer robot is used as the experimental platform. The position and velocity of the robot's end-effector in Cartesian space w.r.t robot base frame can be read directly by the sensor of the robot. A Novint Falcon haptic device is used to measure the magnitude and direction of the human-applied force. The force applied to the haptic device is directly reflected on the robot's end-effector. A monocular camera is used to obtain visual information about the robot and its surroundings. The captured image is displayed on a monitor for human observation, together with the prescribed trajectory and two human desired positions.

For simplicity, the experiment focuses on the motion of one feature point which is the projection of the robot's end-effector on the image plane. The motion of the feature point is displayed on the monitor. When the feature point moves along the prescribed trajectory, the human can apply force to move the feature point to human desired positions. After reaching two human desired positions, the human releases the robot and applies no force. Then the feature point continues to track the prescribed trajectory, finally reaching the target point. The experimental settings are as follows.

The calibrated perspective projection matrix is

$$P = \begin{bmatrix} -310.25 & 584.72 & 34.27 & 381.92 \\ -271.00 & 23.30 & -569.36 & 545.43 \\ -1.00 & 0.02 & 0.05 & 1.25 \end{bmatrix}$$

The starting point and the target point on the image plane are set to $y_s = [160, 275]^T$ and $y_t = [400, 360]^T$, respectively.

Fig. 3. Experimental setup. The actual environment (left) and the image captured by the camera (right)

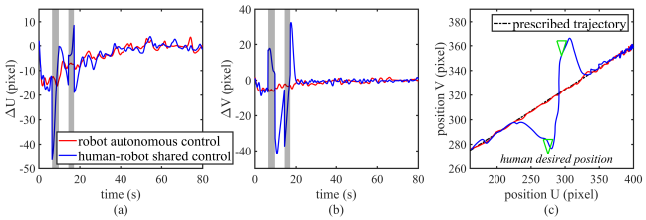

Fig. 4. The tracking error and actual trajectory of the robot in "robot autonomous control"(the first case) and "human-robot shared control"(the second case) conditions. The gray region represents that there is a force applied by the human. (a) The tracking error in the U dimension. (b) The tracking error in the V dimension. (c) Trajectories in the image plane.

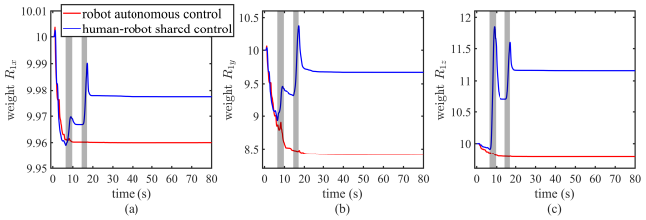

Fig. 5. The robot control weight in "robot autonomous control"(the first case) and "human-robot shared control"(the second case) conditions. The gray region represents that there is a force applied by the human. (a), (b), and (c) represent the x, y, and z dimensions, respectively.

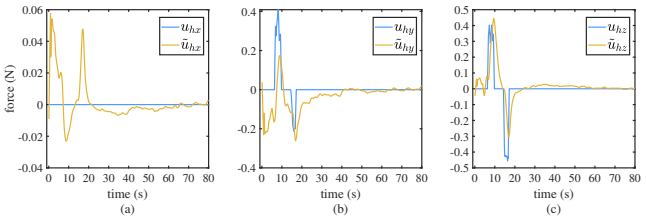

Fig. 6. The force applied by the human and the estimated human force. (a), (b) and (c) represent the x, y and z dimensions, respectively.

The prescribed trajectory is generated by $y_d(t) = [160 + (400-160)\times(1-e^{-\frac{t}{15}}), 275+(360-275)\times(1-e^{-\frac{t}{15}})]^T$. The total run time t_{end} is set to $80s$. Two human desired positions are set to $y_{h1} = [280, 285]^T$, $y_{h2} = [300, 355]^T$. The impedance parameters in (5) are set to $H_d = 3\mathbf{I}_{3\times3}$ kg and $C_d = 10\mathbf{I}_{3\times3}$ Ns/m. The initial values of estimated weights in (21) are set to $\tilde{Q}_1 = 10^{-3}\mathbf{I}_{2\times2}$, $\tilde{Q}_2 = 10^{-5}\mathbf{I}_{2\times2}$, $\tilde{R}_1 = 10\mathbf{I}_{3\times3}$. The weight R_2 is set to $10\mathbf{I}_{3\times3}$. The initial value of the estimated neural network weight $\tilde{W}$ of each neuron is set to 1. The parameters of activation function are set to $\zeta = 10000$, $\rho = 10$ and the learning rates are $\alpha_1 = 100$, $\alpha_2 = 6\times10^{-10}$, $\alpha_3 = 1.2$, $\beta = 5$. For safety, we set the upper and lower boundaries for $\tilde{Q}_1, \tilde{Q}_2, \tilde{R}_1$ as:$[10^{-5}, 10^{-1}]$, $[10^{-7}, 10^{-3}]$, $[10^{-2}, 10^{4}]$, respectively.

B. Adaptation Performance

To evaluate the adaptation performance of the proposed method, we conducted experiments in two cases. In the first case, the human applies no force(the human has no influence in the robot) and the control objective is tracking the prescribed trajectory. In the second case, the human applies force to move the feature point, and the control objective is modified to reach human desired positions.

To analyze the performance of the proposed method, the following criteria are considered:

1) The tracking error: $\delta = y - y_{h1}$ or $y - y_{h2}$ when there is a force applied by the human. Otherwise, $\delta = y - y_d$. The tracking errors in U and V dimensions are respectively presented as ΔU and ΔV.

2) The robot control weight in x, y, and z dimensions as R_{1x}, R_{1y}, and R_{1z}.

3) The force applied by the human in x, y, and z dimensions as u_{hx}, u_{hy}, and u_{hz}. The corresponding estimated human force, as $\tilde{u}_{hx}$, $\tilde{u}_{hy}$, and $\tilde{u}_{hz}$.

In the first case, the human applies no force. The feature point tracks the prescribed trajectory and the robot executes the visual servoing task alone. The results of the tracking error and the robot control weight are shown in Fig. 4 and Fig. 5, respectively. Although there are large tracking errors in both U and V dimensions at the beginning (the maximum errors are 16.2 pixels and 6.3 pixels, respectively) as shown in Fig. 4 (a) and (b), the robot control weights R_{1x}, R_{1y} and R_{1z} shown in Fig. 5 continuously decrease to make the robot take the lead in the task and reduce tracking errors(when the time came to 40s, the tracking errors reduce to 20% and 6.8% of the maximum errors in the U and V dimensions, respectively). Finally, the tracking errors in the U and V dimensions converge to zero.

In the second case, the human applies force to move the feature point to human desired positions. As shown in Fig. 5, at the beginning, the robot control weights R_{1x}, R_{1y} and R_{1z} decrease to make the robot lead the task and reduce the tracking error of the prescribed trajectory. When the human applies force(in y and z dimensions), the robot control weights R_{1y} and R_{1z} obviously increase to make the robot more compliant and make the human lead the task. After the force disappears, the robot control weights R_{1y} and R_{1z} decrease again to reduce the tracking error of the prescribed trajectory. The result in Fig. 6 shows that the estimated human force $\tilde{u}_h$ tries to track the actual human force u_h and the general trend is the same in both the y and z dimensions, which indicates the proposed method estimates human intention correctly.

Based on the above results, we conclude that the proposed method achieves the following performance: 1) when there is no force applied by the human, the robot control weight decreases to make the robot lead the task, minimizing the

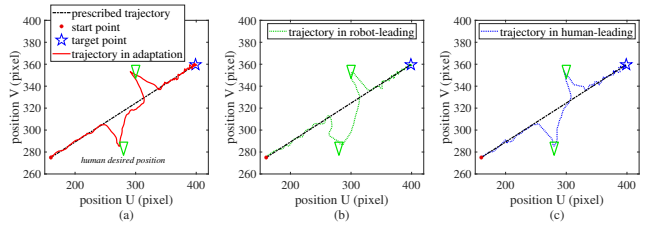

Fig. 7. (a) The actual trajectory in adaptation condition. (b) The actual trajectory in robot-leading condition. (c) The actual trajectory in human-leading condition.

error of tracking the prescribed trajectory and completing the initially given task. 2) When the human applies force, the control objective of the robot is adjusted to reach human desired positions, and the robot control weight increases to make the robot more compliant and make the human lead the task, minimizing the interaction force. 3) The human intention is estimated correctly as the estimated human force tracks the actual human force.

C. User Study

When facing the experiment introduced in Section IV-A, different people may adopt different levels of force to move the feature point to human desired positions. To verify the generality of the proposed method, we conduct a user study.

To compare the performance of our proposed method with the fixed-role control method, we consider the following conditions: 1) "robot-leading", a fixed robot control weight with $R_1 \equiv 10\mathbf{I}_{3\times3}$. 2) "human-leading", a fixed robot control weight with $R_1 \equiv 20\mathbf{I}_{3\times3}$. 3) "adaptation", the proposed method with $R_1(0) = 10\mathbf{I}_{3\times3}$. In these conditions, the human and the robot work together and the system is under shared control. The remaining parameters are set the same as introduced in Section IV-A.

Ten volunteers (age: $\mu = 25.40$, $\sigma = 2.73$) are chosen to participate in this experiment. They are informed of the specific details of the experiment and instructed to use the haptic device. They can practice until they are familiar with the experiment. Eventually, each volunteer conducts two trials for each experimental condition and 20 sets of data are collected in each experimental condition. To clearly compare the experimental results in three experimental conditions, We select a representative set of experiments, and the results are shown in Fig. 7 and Fig. 8.

Fig. 8 (a) shows that, when there is no force applied by the human (0s-7s), the tracking errors in the "adaptation" and "robot-leading" conditions are similar and obviously smaller than that in the "human-leading" condition. Fig. 8(b) and (c) show that though the feature point reaches human desired positions in all three experimental conditions, the force applied by the human and human power in the "robot-leading" condition are larger than those in the "adaptation" and "human-leading" conditions. The above results indicate that by dynamically adjusting the robot control weight, the proposed method can combine the excellent trajectory tracking ability in the fixed-role "robot-leading" condition and

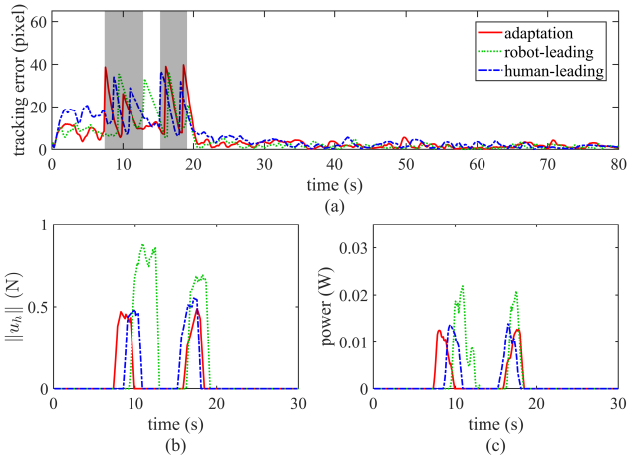

Fig. 8. (a) The tracking error in three experimental conditions, the definition is same as Section IV-B. The gray region represents the largest scale of force applied by the human in three experimental conditions. (b) The norm of the force applied by the human, $\|u_h\|$. (c) The human power in three experimental conditions.

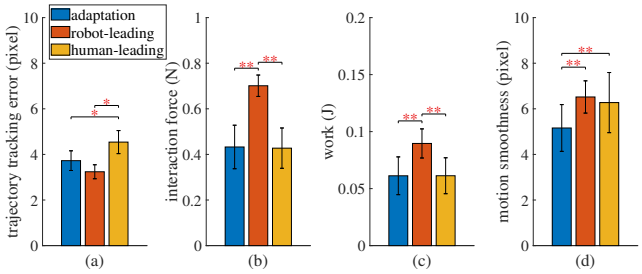

Fig. 9. The statistical analysis of performance in three experimental conditions. (a) The mean trajectory tracking error. (b) the mean interaction force. (c) the work done by the human. (d) the motion smoothness of the robot. A single asterisk "*" means $p < 0.05$ and a double "**" means $p < 0.01$.

the high human-following ability in the fixed-role "human-leading" condition.

To make a statistical analysis of the performance in three experimental conditions, the following measures are considered for each set of data:

1) The mean trajectory tracking error when no force is applied by the human: $\varepsilon = \frac{1}{t_{nf}} \int_{t_{nf}} \|y - y_d\| dt$, t_{nf} denotes the time when there is no force applied by the human.

2) The mean interaction force: $F = \frac{1}{t_f} \int_{t_f} \|u_h\| dt$, t_f denotes the time when the force is applied by the human.

3) The work done by the human to move the feature point to human desired positions: $\omega = \int_0^{t_{end}} {u_h}^T \dot{x} dt$.

4) The motion smoothness. It's calculated by the distance between the upper and lower envelopes of the robot's motion curves. A smaller value of motion smoothness means a smoother trajectory.

The mean and standard deviation of the trajectory tracking error, the interaction force, the work done by the human, and the motion smoothness are calculated using 20 sets of data for each experimental condition. Then, we conduct the one-way analysis of variance (ANOVA) to test the null

hypothesis that there is no difference among the population means of three experimental conditions. To clarify which two experimental conditions have significant differences in the population mean, we further conduct multiple comparisons between any two experimental conditions.

Fig. 9 (a) shows that the null hypothesis is rejected for the mean trajectory tracking error. Specifically, the mean trajectory tracking errors in "adaptation" and "robot-leading" conditions are similar and significantly smaller ($p < 0.05$) than that in the "human-leading" condition.

Fig. 9 (b) shows that the null hypothesis is rejected for the mean interaction force. The mean interaction force in the "adaptation" condition is similar to that in the "human-leading" condition, and significantly smaller than that in the "robot-leading" condition ($p < 0.01$).

Fig. 9 (c) shows that the null hypothesis is rejected for the work done by the human. In particular, the work in "adaptation" and "human-leading" conditions is similar and significantly smaller ($p < 0.01$) than that in the "robot-leading" condition.

Fig. 9 (d) shows that the null hypothesis is rejected for the motion smoothness. The motion smoothness in the "adaptation" condition is significantly smaller ($p < 0.01$) than that in "robot-leading" and "human-leading" conditions.

In conclusion, the results demonstrate that the proposed method can combine the excellent trajectory tracking ability of the "robot-leading" control with the ability to minimize the interaction force and the work done by the human of the "human-leading" control, achieving the best in motion smoothness and outperforming the fixed-role control method.

V. CONCLUSIONS

In this work, we propose a framework of a human-robot shared visual servoing system based on game theory. The radial basis function neural network is designed to estimate human intention, and dynamic role adaption in the human-robot shared visual servoing system is achieved by online updating weights of the cost function. Real experiments are designed to verify the performance of our proposed human-robot shared visual servoing system. The results show that the framework can allow human participation in visual servoing and achieve dynamic role adaptation, outperforming the fixed-role control methods. Future work will consider complex scenes with the uncalibrated camera.

REFERENCES

[1] J. Zhou, Z. Li, X. Li, X. Wang, and R. Song, "Human–robot cooperation control based on trajectory deformation algorithm for a lower limb rehabilitation robot," *IEEE/ASME Transactions On Mechatronics*, vol. 26, no. 6, pp. 3128–3138, 2021.

[2] C. Lu, R. Gao, L. Yin, and B. Zhang, "Human–robot collaborative scheduling in energy-efficient welding shop," *IEEE Transactions on Industrial Informatics*, vol. 20, no. 1, pp. 963–971, 2023.

[3] T. Liu, E. Lyu, J. Wang, and M. Q.-H. Meng, "Unified intention inference and learning for human–robot cooperative assembly," *IEEE Transactions on Automation Science and Engineering*, vol. 19, no. 3, pp. 2256–2266, 2021.

[4] N. Oda, M. Ito, and M. Shibata, "Vision-based motion control for robotic systems," *IEEJ Transactions on Electrical and Electronic Engineering*, vol. 4, no. 2, pp. 176–183, 2009.

[5] D. P. Losey, C. G. McDonald, E. Battaglia, and M. K. O'Malley, "A review of intent detection, arbitration, and communication aspects of shared control for physical human–robot interaction," *Applied Mechanics Reviews*, vol. 70, no. 1, p. 010804, 2018.

[6] Z. Zhuang, Y. Ben-Shabat, J. Zhang, S. Gould, and R. Mahony, "Goferbot: a visual guided human-robot collaborative assembly system," in *2022 IEEE/RSJ International Conference on Intelligent Robots and Systems (IROS)*, pp. 8910–8917, IEEE, 2022.

[7] M. Selvaggio, F. Abi-Farraj, C. Pacchierotti, P. R. Giordano, and B. Siciliano, "Haptic-based shared-control methods for a dual-arm system," *IEEE Robotics and Automation Letters*, vol. 3, no. 4, pp. 4249–4256, 2018.

[8] P. Chang, R. Luo, M. Dorostian, and T. Padır, "A shared control method for collaborative human-robot plug task," *IEEE Robotics and Automation Letters*, vol. 6, no. 4, pp. 7429–7436, 2021.

[9] D. J. Agravante, A. Cherubini, A. Bussy, and A. Kheddar, "Human-humanoid joint haptic table carrying task with height stabilization using vision," in *2013 IEEE/RSJ International Conference on Intelligent Robots and Systems*, pp. 4609–4614, IEEE, 2013.

[10] X. Yu, W. He, Q. Li, Y. Li, and B. Li, "Human-robot co-carrying using visual and force sensing," *IEEE Transactions on Industrial Electronics*, vol. 68, no. 9, pp. 8657–8666, 2020.

[11] M. Ma and L. Cheng, "A human–robot collaboration controller utilizing confidence for disagreement adjustment," *IEEE Transactions on Robotics*, vol. 40, pp. 2081–2097, 2024.

[12] M. Selvaggio, M. Cognetti, S. Nikolaidis, S. Ivaldi, and B. Siciliano, "Autonomy in physical human-robot interaction: A brief survey," *IEEE Robotics and Automation Letters*, vol. 6, no. 4, pp. 7989–7996, 2021.

[13] N. Jarrassé, T. Charalambous, and E. Burdet, "A framework to describe, analyze and generate interactive motor behaviors," *PloS one*, vol. 7, no. 11, p. e49945, 2012.

[14] Y. Li, G. Carboni, F. Gonzalez, D. Campolo, and E. Burdet, "Differential game theory for versatile physical human–robot interaction," *Nature Machine Intelligence*, vol. 1, no. 1, pp. 36–43, 2019.

[15] H. Xia, M. Pi, L. Jin, R. Song, and Z. Li, "Human collaborative control of lower-limb prosthesis based on game theory and fuzzy approximation," *IEEE Transactions on Cybernetics*, vol. 55, no. 1, pp. 247–258, 2025.

[16] L. Han, J. Zhang, and H. Wang, "Shared control in phri: Integrating local trajectory replanning and cooperative game theory," *IEEE Transactions on Robotics*, vol. 41, pp. 1263–1277, 2025.

[17] P. Franceschi, D. Cassinelli, N. Pedrocchi, M. Beschi, and P. Rocco, "Design of an assistive controller for physical human–robot interaction based on cooperative game theory and human intention estimation," *IEEE Transactions on Automation Science and Engineering*, vol. 22, pp. 5741–5756, 2025.

[18] P. Franceschi, N. Pedrocchi, and M. Beschi, "Adaptive impedance controller for human-robot arbitration based on cooperative differential game theory," in *2022 International Conference on Robotics and Automation (ICRA)*, pp. 7881–7887, IEEE, 2022.

[19] Y. Li, K. P. Tee, W. L. Chan, R. Yan, Y. Chua, and D. K. Limbu, "Continuous role adaptation for human–robot shared control," *IEEE Transactions on Robotics*, vol. 31, no. 3, pp. 672–681, 2015.

[20] Y. Li, K. P. Tee, R. Yan, W. L. Chan, and Y. Wu, "A framework of human–robot coordination based on game theory and policy iteration," *IEEE Transactions on Robotics*, vol. 32, no. 6, pp. 1408–1418, 2016.

[21] Y.-H. Liu, H. Wang, C. Wang, and K. K. Lam, "Uncalibrated visual servoing of robots using a depth-independent interaction matrix," *IEEE Transactions on Robotics*, vol. 22, no. 4, pp. 804–817, 2006.

[22] N. Hogan, "Impedance control: An approach to manipulation," in *1984 American control conference*, pp. 304–313, IEEE, 1984.

[23] L. Busoniu, R. Babuska, and B. De Schutter, "A comprehensive survey of multiagent reinforcement learning," *IEEE Transactions on Systems, Man, and Cybernetics, Part C (Applications and Reviews)*, vol. 38, no. 2, pp. 156–172, 2008.

[24] K. G. Vamvoudakis and F. L. Lewis, "Multi-player non-zero-sum games: Online adaptive learning solution of coupled hamilton–jacobi equations," *Automatica*, vol. 47, no. 8, pp. 1556–1569, 2011.

[25] M. Abu-Khalaf and F. L. Lewis, "Nearly optimal control laws for nonlinear systems with saturating actuators using a neural network hjb approach," *Automatica*, vol. 41, no. 5, pp. 779–791, 2005.

[26] K. G. Vamvoudakis and F. L. Lewis, "Online actor–critic algorithm to solve the continuous-time infinite horizon optimal control problem," *Automatica*, vol. 46, no. 5, pp. 878–888, 2010.